nature geoscience

ARTICLES

https://doi.org/10.1038/s41561-020-0565-6

Abundant nitrite-oxidizing metalloenzymes in the mesopelagic zone of the tropical Pacific Ocean

Mak A. Saito[1]✉, Matthew R. McIlvin[1], Dawn M. Moran[1], Alyson E. Santoro[2], Chris L. Dupont[3], Patrick A. Rafter[4], Jaclyn K. Saunders[1], Drishti Kaul[3], Carl H. Lamborg[5], Marian Westley[6], Frederica Valois[1] and John B. Waterbury[1]

Numerous biogeochemical reactions occur within the oceans' major oxygen minimum zones, but less attention has been paid to the open ocean extremities of these zones. Here we report measurements on oxygen minimum zone waters from the Eastern to the Central Tropical North Pacific, which we analysed using metaproteomic techniques to discern the microbial functions present and their influence on biogeochemical cycling. We found nitrite oxidoreductase—an iron-rich enzyme from *Nitrospina* bacteria—to be one of the most abundant microbial proteins present in the mesopelagic zone, with over 60 billion molecules per litre. Estimated reaction rates imply that this enzyme is undersaturated and that its high abundance provides a latent mesopelagic catalytic capacity to rapidly oxidize nitrite derived from episodic fluxes of degrading sinking organic matter. In addition, given the enzyme's intensive iron demand, its high abundance represents a previously unrecognized microbial reservoir within suboxic mesopelagic zones. Nitrite oxidoreductase may also contribute to other reactions involving nitrogen and redox-sensitive metals. We suggest that the abundance and extent of nitrite oxidoreductase may increase with continued deoxygenation in the oceans, and result in increased mesopelagic demand for iron and other potential changes to marine biogeochemical cycles.

Nitrogen is an essential nutrient in marine ecosystems[1], whose oceanic inventory and chemical speciation are controlled by elaborate microbial metalloenzymes that catalyse chemical transformations[2]. These are especially important at mesopelagic depths (~200–1,000 m), where key nitrogen reactions, such as chemolithoautotrophic nitrification, oxidize reduced nitrogen for energy[3,4]. Many nitrogen reactions are prevalent in regions of reduced oxygen availability. For denitrification this is due to nitrate being an important oxidant in heterotrophic respiration. For nitrification the reasons are less clear, but may be related to the sensitivity of the iron–sulfur cluster active centres to oxidation within the enzyme active site[5]. Mass-spectrometry-based metaproteomic measurements can directly examine the relative abundance of these enzyme catalysts in oxygen minimum zones (OMZs)[6]. Previous studies have focused on oxygen-deficient areas, where nitrate can act as an alternative electron acceptor and a diverse range of microbial activities is observed[7,8].

While deoxygenation in coastal waters results in anoxic dead zones and macrofauna mortality[9], less is known about the potential consequences of deoxygenation and suboxia expansion for microbial and biogeochemical processes in the open ocean. Trends for basin-scale ocean deoxygenation have been observed[10,11], while modelling studies vary in their predictive capability[12–14]. Within the upper mesopelagic environment, key microbial remineralization and nutrient recycling reactions occur with the degradation of sinking particulate organic material. With nitrogen-rich proteinaceous material contributing roughly half of the biomass of microbial life, the degradation of proteins to smaller constituents, including peptides, amino acids, urea, ammonia, nitrite and nitrate, is a major mesopelagic activity along with the respiration of reduced carbon[15]. In this study we present global and targeted metaproteomic evidence for the preponderance of nitrite oxidoreductase (Nxr), the metalloenzyme involved in the oxidation of nitrite, within OMZ extremities of the Central Pacific Ocean, and discuss the biogeochemical implications.

Metaproteomic sampling expeditions in the Central Pacific Ocean

Two expeditions conducted in the Central Pacific Ocean formed a T pattern over the low-oxygen plume extending from the Eastern Tropical North Pacific Ocean (Metzyme in October 2011 and ProteOMZ in January–February 2016; Fig. 1a). Equatorial upwelling occurs on and to the south of the Equator[16], with corresponding higher productivity and export[17] and scarce dissolved iron, which limits primary productivity[18]. This region experiences strong zonal currents including strong equatorial jets[19] (Supplementary Fig. 1), which can have unique geochemical characteristics reflecting the influence of denitrification (north and south of the Equator) and organic matter remineralization (along and to the south of the Equator)[20]. The Metzyme stations identified suboxic waters centred on 12° N between 200- and 400-m depths (Fig. 1b, Station 2), consistent with the westward extension of the Eastern Tropical North Pacific Ocean OMZ[21]. Within these suboxic waters $\delta^{15}N_{NO_3}$ and N*, defined as a linear combination of nitrate and phosphate[21,22] (see Methods), showed signals characteristic of denitrification[23], with $\delta^{15}N_{NO_3} > 11‰$ and $N^* < -7\,\mu mol\,kg^{-1}$ (station 2, 12°) notably offset from the surrounding waters (Fig. 1d,j)[16,20], and advected either from the eastern boundary coastal OMZ regions and/or by in situ microbial processes. The subsequent ProteOMZ expedition followed these low-oxygen waters eastward along 10° N as far as 140° W (Fig. 1c) and observed suboxic OMZ waters (<5 μM O_2 at stations 4, 6, 7 and 8) and low N* throughout the mesopelagic (Fig. 1e),

[1]Woods Hole Oceanographic Institution, Woods Hole, MA, USA. [2]University of California, Santa Barbara, CA, USA. [3]J. Craig Venter Institute, La Jolla, CA, USA. [4]University of California, Irvine, CA, USA. [5]University of California, Santa Cruz, CA, USA. [6]National Oceanographic and Atmospheric Administration, Silver Spring, MD, USA. ✉e-mail: msaito@whoi.edu

demonstrating the coherence of these OMZ waters throughout the Eastern Tropical North Pacific Ocean and their distinct nitrogen biogeochemical signals in this region.

Free-living microbial biomass was collected by size-fractionated in situ filtration systems (0.2–3.0-µm pore size range) on seven vertical profiles (Metzyme stations 1, 3, 5 and ProteOMZ 4, 6, 7 and 8). Two metaproteomic techniques, data-dependent acquisition global metaproteomic analyses and targeted metaproteomic analyses, were applied to 77 samples from the profiles (Supplementary Table 1). Metzyme and ProteOMZ samples were analysed by one- and two-dimensional chromatographic methods, respectively, and protein identifications were assigned by spectrum-to-peptide matching to a custom translated metagenomics assembly produced from six sample splits from Metzyme (Supplementary Table 1). Tryptic peptides were identified and enumerated by exclusive spectral counts for subsequent targeted metaproteomic studies as previously described[24]. Custom standards were prepared using heterologous overexpression of stable-isotope-labelled tryptic peptides[25] and used to calibrate the targeted metaproteomic analyses (Supplementary Methods).

An abundant mesopelagic metalloenzyme

A surprising finding was the abundance of Nxr enzyme subunits within the global metaproteome throughout the suboxic mesopelagic depths. Spectral counts for Nxr protein subunits (NxrA and NxrB) were higher than those for than any other protein within the mesopelagic zone at Metzyme station 3 (Fig. 2a) and all other profiles in this region (Supplementary Fig. 2). Nxr protein identifications were supported by multiple peptide identifications: as many as 21 and 13 tryptic peptides for NxrA and NxrB were observed, respectively, corresponding to 34% and 48% protein sequence coverage (Supplementary Fig. 4). It is unlikely that other abundant proteins remain unidentified due to use of paired metagenomic data for spectrum-to-peptide matches. Sequence alignment (Supplementary Figs. 5 and 6) and genome binning (Supplementary Fig. 7) found the identified Nxr peptides to be associated with the nitrite-oxidizing bacterium (NOB) *Nitrospina* from the proposed bacterial phylum Nitrospinae, which are important oceanic nitrite oxidizers[3,26–28]. Metagenomic, metatranscriptomic and metaproteomic analyses have identified *Nitrospina* and its Nxr enzyme within oxygen minimum waters in OMZ regions off coastal Chile[29] and the seasonally anoxic fjord Saanich Inlet[6], and within single amplified genomes of *Nitrospina*[30].

Proteomic analyses of NOB cultures of *Nitrospira marina* and *Nitrococcus mobilis* showed NxrA and NxrB subunits to be among the most abundant proteins in relative abundance spectral counts (Nb-295 in Fig. 2b; Nb-231 in Supplementary Fig. 8). This Nxr abundance is also consistent with previous immunocytological and electron microscopy observations from the NOB *Nitrospira moscoviensis*, where striking lattice membrane features were observed and attributed to the abundant surface Nxr membrane protein complex[31]. The dominance of Nxr proteins in NOB cultures provides a mechanism for the observation of the enzyme's abundance in the mesopelagic ocean.

Absolute abundances of Nxr enzyme subunits by targeted metaproteomics

Targeted metaproteomic assays[24] were used to determine absolute concentrations of Nxr and their stoichiometries. 12 tryptic peptides representing NxrA and NxrB protein subunits were identified in the global proteomic dataset and synthesized as isotopically labelled internal standards by heterologous overexpression (Supplementary Tables 2 and 3). The standards showed linear response in standard curves (Supplementary Fig. 8), chromatographic resolution (Supplementary Figs. 14–25), and low detection limits (Supplementary Table 3). Triplicate analyses for three sample depths had an average of the relative s.d. of 3.9%–6.2% for all 12 peptides (Supplementary Table 4). 11 of the 12 peptides were taxonomically attributed exclusively to the NOB *Nitrospina* sp., with the 12th peptide present in both *Nitrospira* and *Nitrospina* (Supplementary Tables 5 and 6), by least common ancestor analysis using representative NOB genomes and single amplified genomes[24]. The peptides were measured by parallel reaction monitoring (PRM; Supplementary Fig. 9) on a quadrupole–Orbitrap mass spectrometer. Vertical profiles of NxrA and NxrB peptides showed similar trends in distributions (Supplementary Fig. 10), and were averaged for composite NxrA and NxrB subunit abundances (Figs. 3 and 4). While variability in Nxr peptides could stem from analytical or sample processing reproducibility, sequence alignments of the paired metagenomic data showed considerable variation within the targeted peptide regions (Supplementary Figs. 5 and 6), demonstrating the presence of an Nxr enzyme population not easily targeted by a single conserved peptide sequence. Despite this Nxr diversity, the coherence captured by the suite of targeted metaproteomic peptides was surprisingly good.

The greatest abundance of Nxr was observed at Metzyme station 3 at 300 m depth with 107 and 155 fmol l^{-1} for NxrA and NxrB, respectively (relatively close to a 1:1 subunit stoichiometry), equivalent to over 60 billion molecules per litre and 1.3% of the total protein in this size fraction (Fig. 3 and Supplementary Table 7). This percentage of total protein is consistent with Nxr being an abundant protein within NOB cultures (~10% of cellular protein)[31], and NOB abundance in the mesopelagic ocean[3,26–28]. While all seven Pacific vertical profiles showed abundant mesopelagic Nxr subunits, Nxr vertical structure varied considerably by station, with the two subunits generally tracking each other (Fig. 4), implying that Nxr abundance reflects variability in export flux and nitrite supply. Nxr was less abundant than euphotic zone cyanobacterial proteins, which can reach thousands of femtomoles per litre (ref. [32]), due to higher euphotic zone biomass, with total particulate protein four to eight times lower in the mesopelagic versus the euphotic zone (Supplementary Figs. 3 and 12). However, the most abundant euphotic zone proteins were not elementally costly metalloenzymes such as Nxr. Finally, a comparison of Nxr protein abundance with *Nitrospina*-like NOB determined by quantitative DNA analysis showed a positive linear relationship with an r^2 of 0.43 (Supplementary Fig. 12 and Supplementary Table 8), supporting the case for high Nxr in the OMZ due to more NOB, rather than more Nxr per NOB.

The average abundances of Nxr peptides on the ProteOMZ expedition were lower than those on the Metzyme expedition, with maximal concentrations of 30 and 49 fmol l^{-1}, for NxrA and NxrB, respectively, perhaps due to the ProteOMZ expedition occurring during the strong 2015–2016 El Niño event[33]. Warmer surface waters could have increased stratification, decreased nutrient input and export flux, and resulted in less mesopelagic nitrification. Hydrographic data were consistent with this possibility: the 2011 Metzyme station 3 was reoccupied in 2016 (ProteOMZ station 5), and showed similar euphotic zone temperatures but with a deeper mixed layer depth, although corresponding nutrient datasets did not have sufficient depth resolution to observe changes between years (Supplementary Fig. 12). Nxr was also abundant in shallow surface waters of the South Pacific (METZYME station 6 and ProteOMZ stations 10–14; Supplementary Figs. 2 and 13), where nitrite was more abundant. The absence of Nxr over the nitrite maxima was surprising and may reflect an iron limitation of NOB via an inability to complete the biosynthesis of Nxr's iron centres. Alternatively there may be additional NOB diversity in the South Pacific not yet captured by our study, where lack of metagenomic data prevents the peptide-to-spectrum matches needed to identify and quantify proteins.

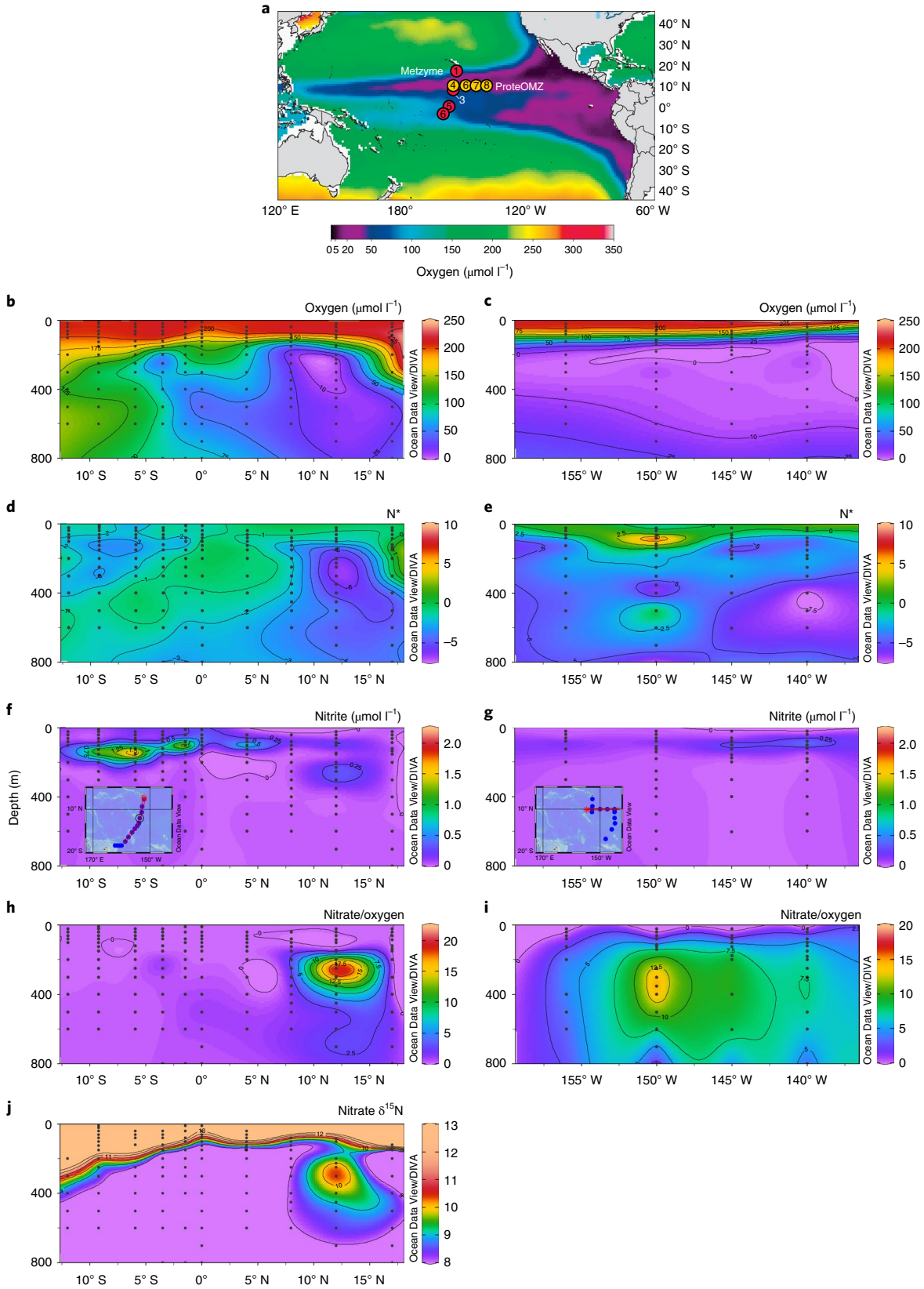

Fig. 1 | Station locations, hydrographic features and Nxr distributions for the Metzyme and ProteOMZ expeditions. a, Profile stations marked in red for Metzyme stations 1, 3, 5 and 6 and in yellow for ProteOMZ stations 4, 6, 7 and 8. **b**–**j**, Sections of dissolved oxygen (**b**,**c**), N* (**d**,**e**), nitrite (**f**,**g**), ratio of nitrate to dissolved oxygen (**h**,**i**) and $\delta^{15}N$ (where $\delta^{15}N = {}^{15}N/{}^{14}N_{sample}/{}^{15}N/{}^{14}N_{reference} - 1$, expressed in per mil by multiplying by 1,000) (**j**) for each expedition in the left- and right-hand panels, respectively.

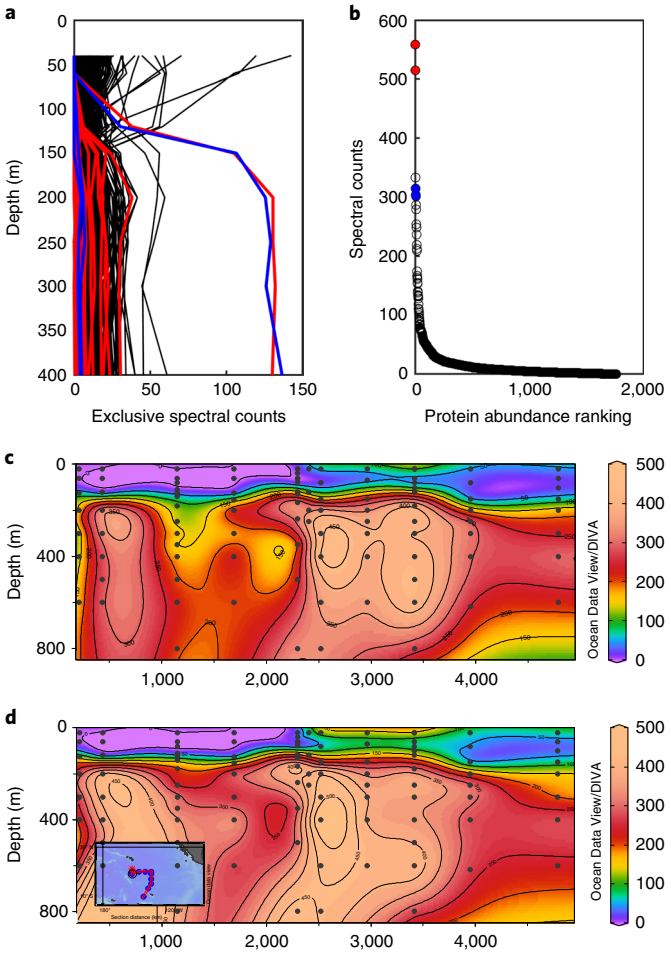

Fig. 2 | Abundant Nxr in the Central Pacific Ocean and in a *Nitrospira* culture. a, Vertical profiles of 3,175 identified proteins from Metyzme station 3 in the Central Pacific Ocean on the basis of global metaproteomic results identified with a paired metagenomic dataset. The NxrA (red) and NxrB (blue) subunits were among the most abundant proteins in the mesopelagic zone by exclusive spectral counting relative abundance measurements. Multiple Nxr lines represent the diversity of Nxr sequences in the metagenome. Despite exclusive spectral counting restricting mapping of each Nxr peptide to one of the diverse Nxr metagenomic sequences, they were clearly highly abundant in the metaproteome. **b**, A ranked protein abundance of the 1,759 proteins identified in the proteome of cultured isolate *N. marina* Nb-295. NxrA (red symbols) ranked 1, 2 and 6; NxrB (blue symbols) ranked 4, 5 and 7; each was among the most abundant proteins in the proteome. **c**,**d**, NxrA (**c**) and NxrB (**d**) subunits on the ProteOMZ expedition, represented in relative abundance total spectral count units. Multiple peptides map to the sequences, as shown in Supplementary Fig. 4.

Iron and Nxr

High Nxr abundance implies a specific microbial iron demand: the Nxr protein complex is an iron–sulfur molybdoprotein whose dimeric form binds 23 atoms of Fe and 1 atom of Mo as determined by enzyme purification[34], although no structure exists as of yet for Nxr. Averaged NxrA and NxrB composite values multiplied by the iron stoichiometry produce an Nxr iron demand profile, assuming that each enzyme was fully metallated (Figs. 3 and 4 and Supplementary Fig. 10), with a maximum concentration of 3.0 ± 0.8 pM Fe as Nxr at Metzyme station 3, and 0.9 ± 0.3 pM Fe as Nxr on the ProteOMZ expedition at station 7 (Figs. 3 and 4). In the oceanic Pacific Ocean, dissolved iron concentrations range from tens to hundreds picomolar and particulate iron ranges from 100 pM near the surface to 500 pM in the mesopelagic. However recent studies showed that the majority (80–100%) of particulate iron consists of non-biological lithogenic material, and hence Nxr could represent an important labile particulate reservoir[35]. Molybdenum within Nxr was less abundant due to its lower stoichiometry (0.12 and 0.035 pM Mo as Nxr at the stations above respectively). With its large oceanic inventory and long residence time, Mo within Nxr probably has a small role in the Mo biogeochemical cycle, although Nxr probably explains the small dissolved Mo variation observed in the mesopelagic Pacific Ocean[36]. While little is known about the mortality of NOB in the mesopelagic, any grazing or viral lysis could result in a flux of dissolved or colloidal Fe and Mo bound within protein constituents.

Role(s) of Nxr in the mesopelagic ocean

The extraordinary abundances of Nxr in the mesopelagic metaproteome probably reflect efforts to maximize cellular contact efficiency with scarce environmental nitrite. Nitrite produced from remineralized sinking organic matter is typically rapidly depleted by these chemolithotrophic NOB to produce energy and fix carbon. Both expeditions observed primary nitrite maxima at depths shallower than 200 m, and a secondary nitrite maximum was observed at 200–300 m in the heart of the OMZ (exceeding 0.5 µM; Metzyme station 2, 12° N, Fig. 1f). Approaching the euphotic zone, the ability of NOB to synthesize Nxr, and thereby oxidize nitrite, may become increasingly challenged by scarce iron availability, particularly in these equatorial regions where scarce iron is limiting to phytoplankton[18]. The accumulation of nitrite, particularly in the South Pacific Subtropical Gyre observed on this transect (Fig. 1f,g), may be related to regional iron scarcity[37], consistent with the distribution of cyanobacterial iron stress biomarkers on this same transect[32].

Another possible role for Nxr's mesopelagic abundance is in catalysing the reverse reaction of nitrate reduction within the OMZ. While it is assumed that O_2 must be depleted before the use of NO_3 as an electron acceptor, the thermodynamic yield from oxidation of organic matter using nitrate is only slightly less than that using oxygen. Moreover, the energy yield for an NOB is far greater from heterotrophic nitrate reduction than from chemolithotrophic NO_2 oxidation. There is some evidence to support this possibility. First, some cultures of NOB[38] and purified Nxr[34] can conduct both nitrate reduction and nitrite oxidation[39], and NxrA and NxrB sequences are homologous with nitrate reductase (NarG and NarH)[40], although presumably some membrane and proteome reorganization would be required to switch between substrates. Second, the ratio of nitrate to dissolved oxygen within this extremity of the OMZ reached 20 and 55 in the Metzyme and ProteOMZ expeditions, respectively (Fig. 1h,i). Third, rapid interconversion between nitrite and nitrate has been observed using nitrite isotopes in the Pacific Ocean and Arabian Sea[41,42], and a nitrate isotopic signal consistent with denitrification was observed in this region as described above (Fig. 1j). Future studies could also explore the potential role of Nxr in reduction reactions found in OMZs, such as those of mercury, iron, chromium and iodine[43–45].

Estimated reaction rates

Potential biogeochemical reaction rates were calculated using Nxr concentrations and specific activity to generate 'omics'-based rate estimates. Several approaches were used based on available kinetic and substrate data (Table 1). First, multiplying the maximum abundance of NxrAB (131 fmol l^{-1}, Metzyme station 3, 300 m; Supplementary Table 7) by the specific activity of purified Nxr from *Nitrobacter hamburgensis*[34] yielded a rate for nitrite oxidation of 85 nM d^{-1} (and a nitrate reduction rate of 59 nM d^{-1}) These are maximum potential reaction rates because they assume saturated substrate abundance; however, this environment is probably

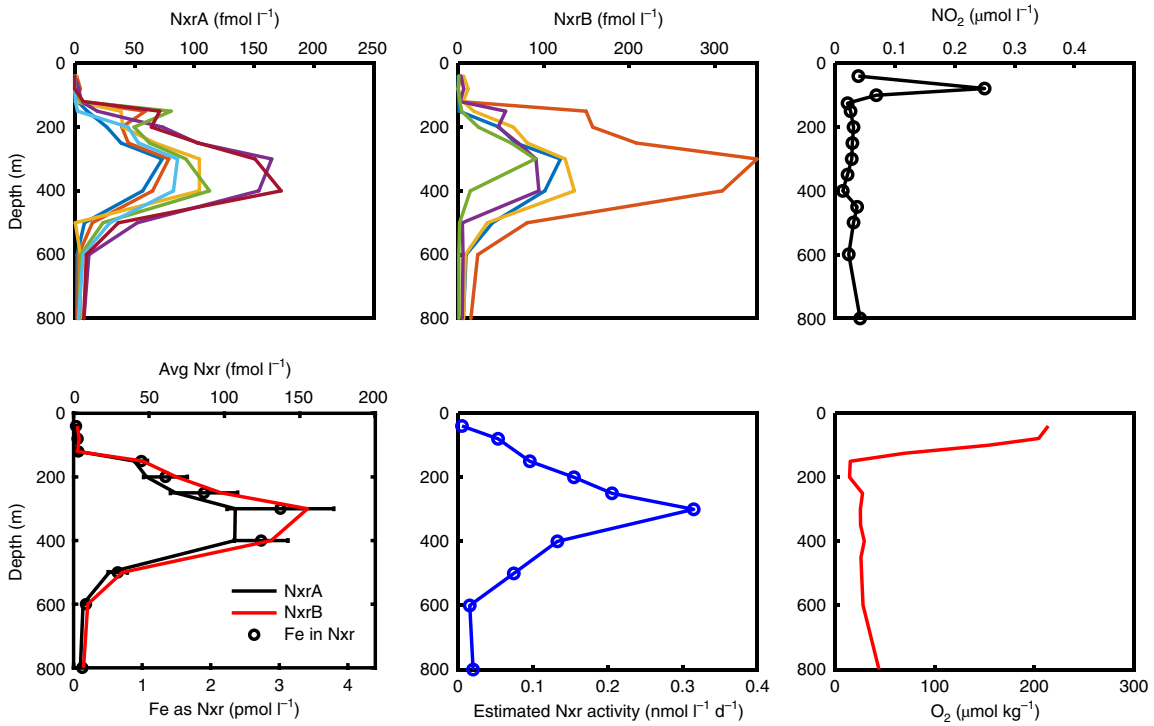

Fig. 3 | Targeted metaproteomic analyses of peptides from Nxr at Metzyme station 3. Vertical profiles of peptides within the NxrA and NxrB proteins, their averages, calculated Fe demand within the Nxr complex, estimated Nxr activity, and nitrite and oxygen vertical profiles. Error bars represent the s.d. associated with the averaged NxrA and NxrB abundances.

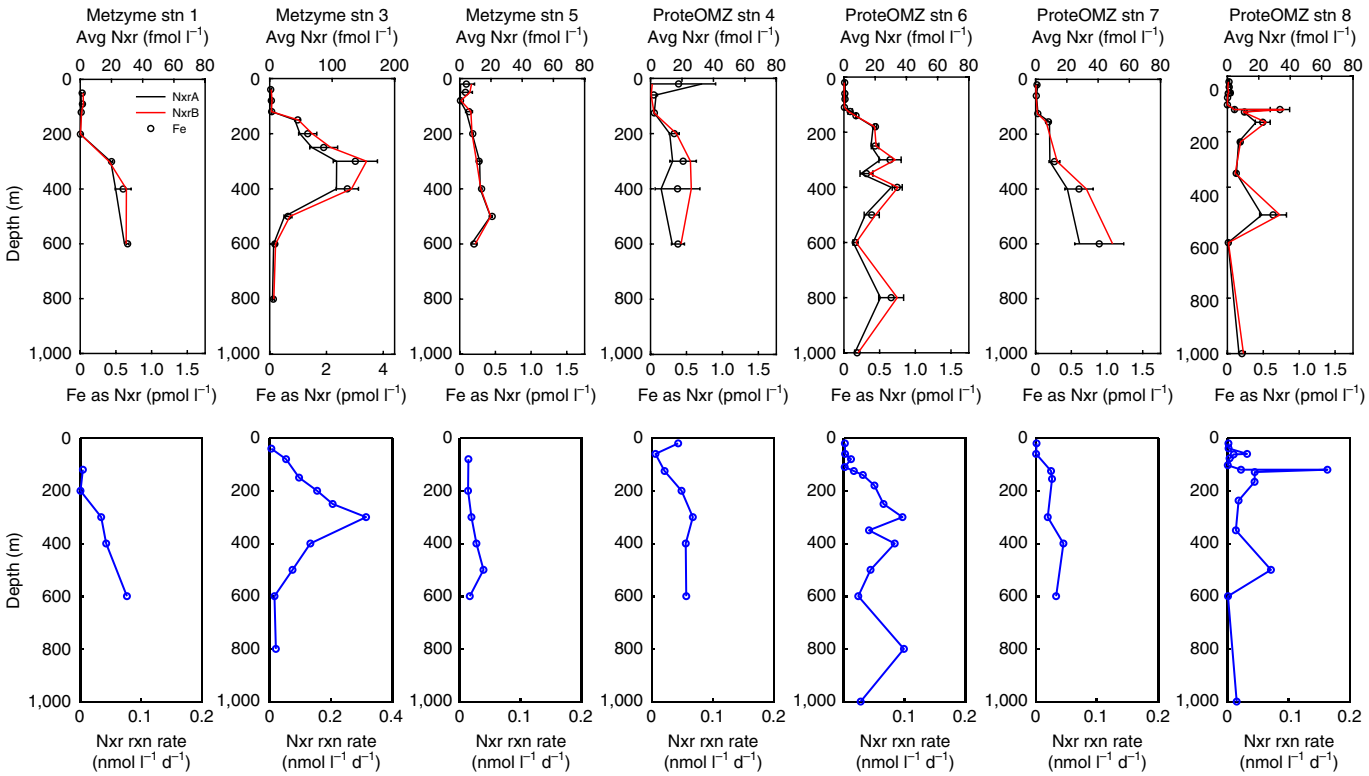

Fig. 4 | Nxr enzyme concentrations, iron use and estimated reaction rates based on targeted metaproteomic analyses. Top row: vertical profiles of subunits NxrA (seven unique peptides) and NxrB (five unique peptides, see Supplementary Table 2) at Metzyme stations 1, 3 and 5 and ProteOMZ stations 4, 6, 7 and 8. Averages of peptides from NxrA and NxrB showed similar distributions and the estimated iron demand associated with this enzyme was calculated from the average of NxrA and NxrB abundances. Error bars represent the s.d. associated with the averaged NxrA and NxrB abundances. Bottom row: estimated reaction rates calculated using average Nxr concentrations, specific activity and nitrite abundances.

Table 1 | Ranges of potential nitrite oxidation reaction rates determined using observed Nxr enzyme concentrations and kinetic parameters from purified protein or cultures

Approach	NO_2 oxidation rate
Calculated using specific activity of purified Nxr (a maximum rate that assumes saturated [NO_2^-])	85 nM d^{-1}
Calculated using Michaelis–Menten kinetics from cultures and the maximum observed nitrite of 0.5 µM	5–6 nM d^{-1}
Calculated using Michaelis–Menten kinetics from cultures and ambient nitrite from vertical profiles	0–0.3 nM d^{-1}
For comparison: isotopic nitrification rates (ammonia oxidation) at Metzyme stations 1, 3 and 5[48]	5–34 nM d^{-1}

substrate limited by nitrite availability. To improve on these estimates, Michaelis–Menten kinetic parameters from whole live cells of *Nitrospina watsonii*[46] and *N. moscoviensis*[47] were paired with the highest nitrite concentration observed on these expeditions (0.5 µM at Metzyme station 2, within the heart of the OMZ of that expedition), yielding upper estimates for the nitrite oxidation rate of 5–6 nM d^{-1} using this relatively high nitrite abundance value. This approach was extended to the seven profiles using averaged NxrAB and nitrite concentrations for each depth (Supplementary Table 9), and kinetic parameters for *N. watsonii*[46]. Profiles of nitrite oxidation rates resembled the Nxr profiles, ranging from zero to 0.3 nM d^{-1} (Figs. 3 and 4), and are probably more representative of actual rates under the lower steady-state nitrite concentrations. The range from steady-state to maximal potential rates probably represents the envelope of possible Nxr activity, where episodic sinking fluxes could intermittently increase nitrite inputs and Nxr rates. These rates compare favourably with concurrently measured nitrification rates (oxidation of ammonia all the way to nitrate), with maximal rates of 5, 5 and 34 nM d^{-1} measured at Metzyme stations 1, 3 and 5, respectively[48], and with modelling studies predicting ~5 nM d^{-1} of ammonia and subsequent nitrite oxidation in the Central North Pacific[49]. These potential reaction rates imply that the mesopelagic ecosystem has the enzymatic capacity to rapidly oxidize nitrite fluxes that result from episodic carbon flux into the mesopelagic ocean.

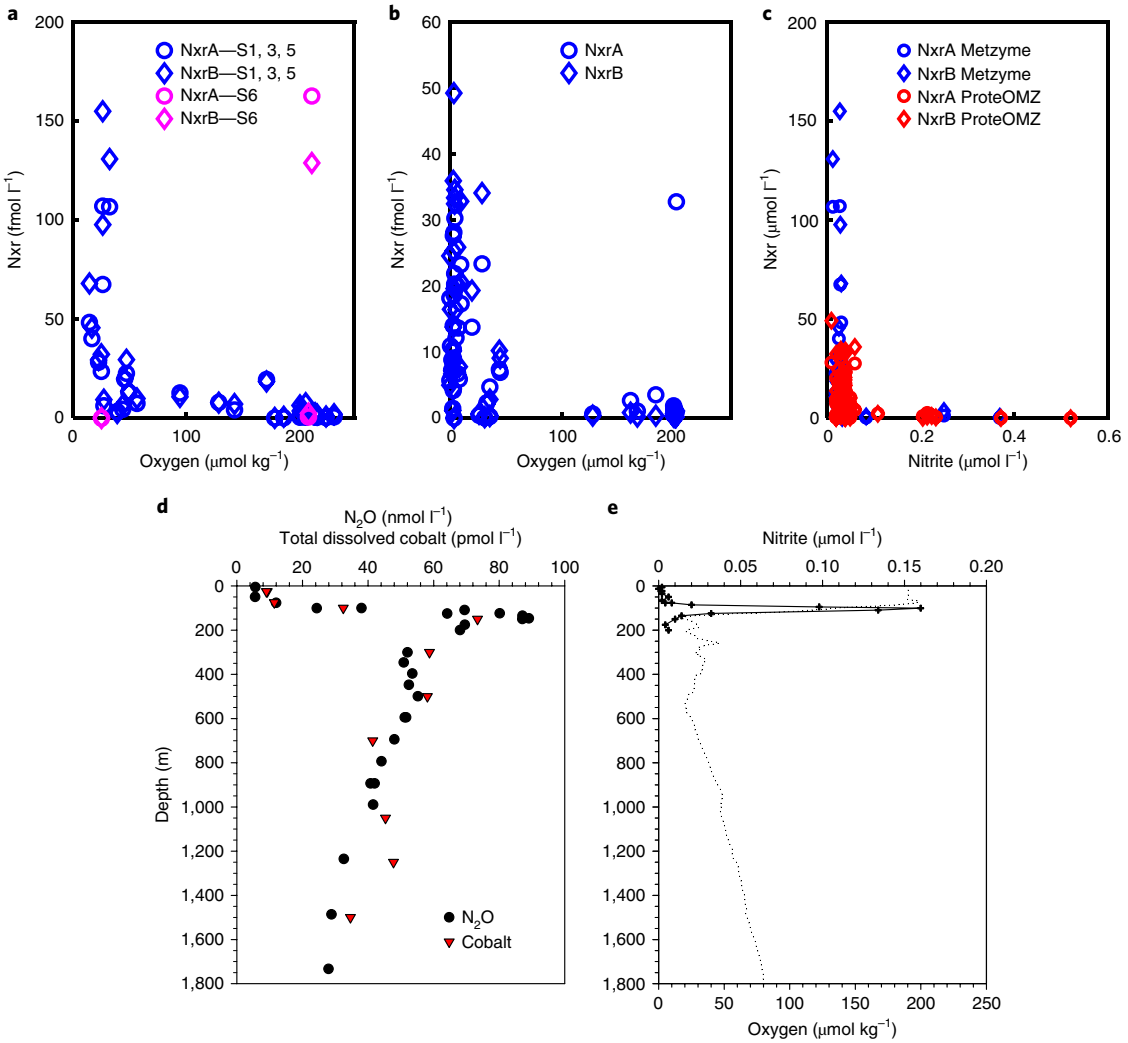

Fig. 5 | Nxr, oxygen and nitrous oxide in the Central Pacific OMZ. a–c, Comparison of NxrA and NxrB subunits (average of seven and five peptides, respectively) with oxygen abundance in Metzyme (**a**) and ProteOMZ (**b**) expeditions, and relationship of NO_2^- and oxygen (**c**). **d**, Nitrous oxide was present near Metzyme station 3 and ProteOMZ station 4 on a previous expedition (RV *Kilo Moana* expedition KM0405 station 5, 8° N 158° W, 28 February 2004). Dissolved cobalt showed a similar vertical structure to N_2O, while being 1,000 times lower in abundance. **e**, Distributions of nitrite (solid) and oxygen (dashed; KM0405 station 5).

These calculated rates assume that oxygen was not limiting nitrite oxidation, yet notably Nxr was abundant when oxygen was low on both expeditions and where nitrite was depleted (Fig. 5a–c). Oxygen scarcity could impede nitrite oxidation and explain the accumulation of nitrite within the OMZ to ~0.5 µM observed during the Metzyme expedition (station 2), although nitrite oxidation has been observed at low oxygen[50]. There are four non-mutually-exclusive explanations for the low-oxygen–high-Nxr trend: (1) higher organic matter and resultant nitrite flux within OMZ regions, (2) greater Nxr persistence due to slowed oxygen degradation of Nxr iron–sulfur clusters (although cultured nitrifiers can be grown aerobically and Nxr was observed at high O_2 in the southern hemisphere as mentioned above), (3) use of Nxr in partial denitrification when NO_3^- is more abundant than O_2, as described above, and (4) an increase in Nxr per NOB cell to compensate for lower oxygen abundance. The linear relationship between Nxr and *Nitrospina*-like NOB described above implies that the high Nxr in the OMZ is due to more NOB, rather than this fourth scenario of more Nxr per NOB.

Implications

This discovery of abundant Nxr in mesopelagic waters offers several new perspectives on these understudied environments. First, while the importance of trace metal nutrition to mesopelagic microbial communities has been explored for copper[4,51,52], these results imply that expansion of suboxic regions by deoxygenation could result in an increased microbial mesopelagic iron demand. Iron is depleted in the euphotic zone of the equatorial and South Pacific. An inability to complete Nxr synthesis could become a constraining factor at the interface with mesopelagic depths when iron is scarce. Some phytoplankton also utilize nitrite[53], but this also requires the iron metalloenzyme ferredoxin–nitrite reductase. The dependence of both nitrite utilization and oxidation on iron availability could explain the prevalence of the extensive nitrite maximum in the South Pacific (Fig. 1f,g)[37]. These findings could have implications for possible unintended consequences of ocean iron fertilization carbon sequestration efforts[54], which may increase carbon, nitrogen and iron fluxes to the mesopelagic, reducing oxygen, probably increasing Nxr abundances and possibly increasing the greenhouse gas N_2O. N_2O is present in these Central North Pacific OMZ extremities below the oxygen clines and nitrite maximum (Fig. 5d,e), and ammonia-oxidizing archaea[55] and NOB[39] were recently shown to produce N_2O, albeit through unknown mechanisms. Any eventual impacts are difficult to predict, as the myriad of interrelated processes that control the mesopelagic ecosystem and their dynamic nature are only beginning to be understood. Together these results demonstrate that the iron metalloenzyme Nxr is highly abundant in the mesopelagic central Pacific Ocean, with a potential activity that appears capable of responding to episodic fluxes, making it an important component of the ecology and biogeochemistry of these environments.

Online content

Any methods, additional references, Nature Research reporting summaries, source data, extended data, supplementary information, acknowledgements, peer review information; details of author contributions and competing interests; and statements of data and code availability are available at https://doi.org/10.1038/s41561-020-0565-6

Received: 3 July 2019; Accepted: 6 March 2020;
Published online: 4 May 2020

References

1. Moore, J. K., Doney, S. C. & Lindsay, K. Upper ocean ecosystem dynamics and iron cycling in a global three-dimensional model. *Global Biogeochem. Cycles* **18**, GB4028 (2004).
2. Voss, M. et al. The marine nitrogen cycle: recent discoveries, uncertainties and the potential relevance of climate change. *Philos. Trans. R. Soc. B* **368**, 20130121 (2013).
3. Watson, S. W. & Waterbury, J. B. Characteristics of two marine nitrite oxidizing bacteria, *Nitrospina gracilis nov. gen. nov. sp.* and *Nitrococcus mobilis nov. gen. nov. sp. Arch. Mikrobiol.* **77**, 203–230 (1971).
4. Ward, B. B. et al. Organic carbon, and not copper, controls denitrification in oxygen minimum zones of the ocean. *Deep Sea Res. I* **55**, 1672–1683 (2008).
5. Imlay, J. A. Iron-sulphur clusters and the problem with oxygen. *Mol. Microbiol.* **59**, 1073–1082 (2006).
6. Hawley, A. K., Brewer, H. M., Norbeck, A. D., Paša-Tolić, L. & Hallam, S. J. Metaproteomics reveals differential modes of metabolic coupling among ubiquitous oxygen minimum zone microbes. *Proc. Natl Acad. Sci. USA* **111**, 11395–11400 (2014).
7. Lam, P. et al. Revising the nitrogen cycle in the Peruvian oxygen minimum zone. *Proc. Natl Acad. Sci. USA* **106**, 4752–4757 (2009).
8. Ward, B., Glover, H. & Lipschultz, F. Chemoautotrophic activity and nitrification in the oxygen minimum zone off Peru. *Deep Sea Res. A* **36**, 1031–1051 (1989).
9. McCormick, L. R. & Levin, L. A. Physiological and ecological implications of ocean deoxygenation for vision in marine organisms. *Philos. Trans. R. Soc. A* **375**, 20160322 (2017).
10. Beman, J. M. et al. Global declines in oceanic nitrification rates as a consequence of ocean acidification. *Proc. Natl Acad. Sci. USA* **108**, 208–213 (2010).
11. Stramma, L., Johnson, G. C., Sprintall, J. & Mohrholz, V. Expanding oxygen-minimum zones in the tropical oceans. *Science* **320**, 655–658 (2008).
12. Keeling, R. F., Körtzinger, A. & Gruber, N. Ocean deoxygenation in a warming world. *Annu. Rev. Mar. Sci.* **2**, 199–229 (2010).
13. Deutsch, C., Brix, H., Ito, T., Frenzel, H. & Thompson, L. Climate-forced variability of ocean hypoxia. *Science* **333**, 336–339 (2011).
14. Fu, W., Primeau, F., Moore, J. K., Lindsay, K. & Randerson, J. T. Reversal of increasing tropical ocean hypoxia trends with sustained climate warming. *Global Biogeochem. Cycles* **32**, 551–564 (2018).
15. Orsi, W. D. et al. Diverse, uncultivated bacteria and archaea underlying the cycling of dissolved protein in the ocean. *ISME J.* **10**, 2158–2173 (2016).
16. Rafter, P. A. & Sigman, D. M. Spatial distribution and temporal variation of nitrate nitrogen and oxygen isotopes in the upper equatorial Pacific Ocean. *Limnol. Oceanogr.* **61**, 14–31 (2016).
17. Barber, R. T. et al. Primary productivity and its regulation in the equatorial Pacific during and following the 1991–1992 El Niño. *Deep Sea Res. II* **43**, 933–969 (1996).
18. Coale, K. H., Fitzwater, S. E., Gordon, R. M., Johnson, K. S. & Barber, R. T. Control of community growth and export production by upwelled iron in the equatorial Pacific Ocean. *Nature* **379**, 621–624 (1996).
19. Johnson, G. C., McPhaden, M. J. & Firing, E. Equatorial Pacific Ocean horizontal velocity, divergence, and upwelling. *J. Phys. Oceanogr.* **31**, 839–849 (2001).
20. Rafter, P. A., Sigman, D. M., Charles, C. D., Kaiser, J. & Haug, G. H. Subsurface tropical Pacific nitrogen isotopic composition of nitrate: biogeochemical signals and their transport. *Global Biogeochem. Cycles* **26**, GB1003 (2012).
21. Gruber, N. & Sarmiento, J. L. Global patterns of marine nitrogen fixation and denitrification. *Global Biogeochem. Cycles* **11**, 235–266 (1997).
22. Deutsch, C., Gruber, N., Key, R. M., Sarmiento, J. L. & Ganachaud, A. Denitrification and N_2 fixation in the Pacific Ocean. *Global Biogeochem. Cycles* **15**, 483–506 (2001).
23. Cline, J. & Kaplan, I. Isotopic fractionation of dissolved nitrate during denitrification in the eastern tropical North Pacific Ocean. *Mar. Chem.* **3**, 271–299 (1975).
24. Saito, M. A. et al. Needles in the blue sea: sub-species specificity in targeted protein biomarker analyses within the vast oceanic microbial metaproteome. *Proteomics* **15**, 3521–3531 (2015).
25. Scott, K. B., Turko, I. V. & Phinney, K. W. Quantitative performance of internal standard platforms for absolute protein quantification using multiple reaction monitoring-mass spectrometry. *Anal. Chem.* **87**, 4429–4435 (2015).
26. Lücker, S., Nowka, B., Rattei, T., Spieck, E. & Daims, H. The genome of *Nitrospina gracilis* illuminates the metabolism and evolution of the major marine nitrite oxidizer. *Front. Microbiol.* **4**, 27 (2013).
27. Santoro, A. E., Casciotti, K. L. & Francis, C. A. Activity, abundance and diversity of nitrifying archaea and bacteria in the central California Current. *Environ. Microbiol.* **12**, 1989–2006 (2010).
28. Füssel, J. et al. Nitrite oxidation in the Namibian oxygen minimum zone. *ISME J.* **6**, 1200–1209 (2012).
29. Stewart, F. J., Ulloa, O. & DeLong, E. F. Microbial metatranscriptomics in a permanent marine oxygen minimum zone. *Environ. Microbiol.* **14**, 23–40 (2012).
30. Ngugi, D. K., Blom, J., Stepanauskas, R. & Stingl, U. Diversification and niche adaptations of *Nitrospina*-like bacteria in the polyextreme interfaces of Red Sea brines. *ISME J.* **10**, 1383–1399 (2016).

31. Spieck, E., Ehrich, S., Aamand, J. & Bock, E. Isolation and immunocytochemical location of the nitrite-oxidizing system in *Nitrospira moscoviensis*. *Arch. Microbiol.* **169**, 225–230 (1998).
32. Saito, M. A. et al. Multiple nutrient stresses at intersecting Pacific Ocean biomes detected by protein biomarkers. *Science* **345**, 1173–1177 (2014).
33. Yin, J., Overpeck, J., Peyser, C. & Stouffer, R. Big jump of record warm global mean surface temperature in 2014–2016 related to unusually large oceanic heat releases. *Geophys. Res. Lett.* **45**, 1069–1078 (2018).
34. Meincke, M., Bock, E., Kastrau, D. & Kroneck, P. M. Nitrite oxidoreductase from *Nitrobacter hamburgensis*: redox centers and their catalytic role. *Arch. Microbiol.* **158**, 127–131 (1992).
35. Ohnemus, D. C. et al. Elevated trace metal content of prokaryotic communities associated with marine oxygen deficient zones. *Limnol. Oceanogr.* **62**, 3–25 (2017).
36. Collier, R. W. Molybdenum in the Northeast Pacific Ocean 1. *Limnol. Oceanogr.* **30**, 1351–1354 (1985).
37. Santoro, A. et al. Measurements of nitrite production in and around the primary nitrite maximum in the central California Current. *Biogeosciences* **10**, 7395–7410 (2013).
38. Spieck, E. et al. Two-dimensional structure of membrane-bound nitrite oxidoreductase from *Nitrobacter hamburgensis*. *J. Struct. Biol.* **117**, 117–123 (1996).
39. Füssel, J. et al. Adaptability as the key to success for the ubiquitous marine nitrite oxidizer *Nitrococcus*. *Sci. Adv.* **3**, e1700807 (2017).
40. Lücker, S. et al. A *Nitrospira* metagenome illuminates the physiology and evolution of globally important nitrite-oxidizing bacteria. *Proc. Natl Acad. Sci. USA* **107**, 13479–13484 (2010).
41. Buchwald, C. & Casciotti, K. L. Isotopic ratios of nitrite as tracers of the sources and age of oceanic nitrite. *Nat. Geosci.* **6**, 308–313 (2013).
42. Buchwald, C., Santoro, A. E., Stanley, R. H. & Casciotti, K. L. Nitrogen cycling in the secondary nitrite maximum of the eastern tropical North Pacific off Costa Rica. *Global Biogeochem. Cycles* **29**, 2061–2081 (2015).
43. Rue, E. R., Smith, G. J., Cutter, G. A. & Bruland, K. W. The response of trace element redox couples to suboxic conditions in the water column. *Deep Sea Res. II* **44**, 113–134 (1997).
44. Moffett, J. W., Goepfert, T. J. & Naqvi, S. W. A. Reduced iron associated with secondary nitrite maxima in the Arabian Sea. *Deep Sea Res. I* **54**, 1341–1349 (2007).
45. Munson, K. M., Lamborg, C. H., Swarr, G. J. & Saito, M. A. Mercury species concentrations and fluxes in the Central Tropical Pacific Ocean. *Global Biogeochem. Cycles* **29**, 656–676 (2015).
46. Jacob, J. et al. Oxidation kinetics and inverse isotope effect of marine nitrite-oxidizing isolates. *Aquat. Microb. Ecol.* **80**, 289–300 (2017).
47. Nowka, B., Daims, H. & Spieck, E. Comparison of oxidation kinetics of nitrite-oxidizing bacteria: nitrite availability as a key factor in niche differentiation. *Appl. Environ. Microbiol.* **81**, 745–753 (2015).
48. Santoro, A. E. et al. Thaumarchaeal ecotype distributions across the equatorial Pacific Ocean and their potential roles in nitrification and sinking flux attenuation. *Limnol. Oceanogr.* **62**, 1984–2003 (2017).
49. Zakem, E. J. et al. Ecological control of nitrite in the upper ocean. *Nat. Commun.* **9**, 1206 (2018).
50. Bristow, L. A. et al. Ammonium and nitrite oxidation at nanomolar oxygen concentrations in oxygen minimum zone waters. *Proc. Natl Acad. Sci. USA* **113**, 10601–10606 (2016).
51. Granger, J. & Ward, B. B. Accumulation of nitrogen oxides in copper limited cultures of denitrifying bacteria. *Limnol. Oceanogr.* **48**, 313–318 (2003).
52. Jacquot, J. E. et al. Assessment of the potential for copper limitation of ammonia oxidation by Archaea in a dynamic estuary. *Mar. Chem.* **162**, 37–49 (2014).
53. Suzuki, I., Sugiyama, T. & Omata, T. Primary structure and transcriptional regulation of the gene for nitrite reductase from the cyanobacterium *Synechococcus PCC 7942*. *Plant Cell Physiol.* **34**, 1311–1320 (1993).
54. Chisholm, S. W., Falkowski, P. & Cullen, J. J. Dis-crediting ocean fertilization. *Science* **294**, 309–310 (2001).
55. Santoro, A. E., Buchwald, C., McIlvin, M. R. & Casciotti, K. L. Isotopic signature of N_2O produced by marine ammonia-oxidizing archaea. *Science* **333**, 1282–1285 (2011).

Methods

Expeditions. Two research expeditions were conducted in the Central Pacific Ocean forming a T pattern over the low-oxygen plume extending from the Eastern Tropical North Pacific Ocean. Metzyme occurred in October 2011 on the RV *Kilo Moana* (KM1128; chief scientists C. Lamborg and M. Saito) and ProteOMZ occurred in January–February 2016 on the RV *Falkor* (FK160115; chief scientist M. Saito). The expedition map is shown in Fig. 1a, and expedition metadata and repository information are available in Supplementary Table 1.

Metaproteomic extraction. *Protein extraction.* Proteins from quarter sections of 142-mm 0.2-µm Supor filters (Pall) were extracted using a modified magnetic bead method from ref. [56]. Filter sections were placed in 5 ml of protein extraction buffer (50 mM HEPES at pH 8.5 (Boston BioProducts), 1% SDS in HPLC-grade water). All reagents in this protocol are made with HPLC-grade water. Samples were heated at 95 °C for 10 min and shaken at room temperature for 30 min. Supor filters were removed and protein extracts were filtered through 5.0-µm Millex low-protein-binding filters (Merck Millipore). Millex filters were rinsed with 1 ml of extraction buffer to insure no loss of protein. Samples were then spun for 30 min at 3,220 *g* in an Eppendorf 5810 centrifuge. The supernatant was removed from the pellet and transferred to a Vivaspin 5,000 MWCO ultrafiltration unit (Sartorius Stedim). Protein extract was concentrated to approximately 350 µl, washed with 1 ml of lysis buffer and transferred to a 2 ml ethanol-washed microtube (all tubes from this point on are ethanol washed). Vivaspins were rinsed with small volumes of protein extraction buffer to remove all concentrated protein, and samples were brought up to 430 µl. An amount of 30 µl was set aside for total protein quantification.

Protein quantification. Standard curves were generated using an albumin standard (Thermo Scientific). Total protein was quantified after extraction and after purification with 2 µl samples in duplicate using the bicinchoninic acid method (Thermo Scientific Micro BCA protein assay kit). Absorbance was measured on a Nanodrop ND-1000 spectrophotometer (Thermo Scientific).

Protein reduction and alkylation. Benzonase nuclease (50 units, 2 µl, Novagen) was added to each sample and incubated at 37 °C for 30 min. Samples were reduced by adding 20 µl of 200 mM dithiothreitol (Fisher) in 50 mM HEPES at pH 8.5 for 30 min at 45 °C. Samples were alkylated by adding 40 µl of 400 mM iodoacetamide (Acros) in HEPES at pH 8.5 for 30 min at 24 °C, occasionally heating to 37 °C to prevent precipitation. The reaction was quenched by adding 40 µl of 200 mM dithiothreitol in 50 mM HEPES at pH 8.5.

Protein purification and digestion. SpeedBeads magnetic carboxylate modified particles (GE Healthcare) were prepared according to ref. [56]. Magnetic beads (20 µl, 20 µg µl^{-1}) were added to 400 µl of extracted protein sample. Samples were heated at 37 °C periodically to avoid precipitation. Samples were acidified to a pH of 2–3 by adding 50 µl of 10% formic acid. Twice the volume (1,100 µl) of acetonitrile was immediately added. Samples were incubated at 37 °C for 15 min and then at room temperature for 30 min. They were then placed on a magnetic rack and incubated for 2 min, and supernatant was removed and discarded. Samples were washed twice, removing and discarding supernatants with 1,400 µl of 70% ethanol for 30 s on the magnetic rack. Acetonitrile (1,400 µl) was added to each sample for 30 s on the magnetic rack. Supernatant was removed and discarded. Samples were air dried for approximately 4 min until the acetonitrile had just evaporated. Samples were removed from the magnetic rack and beads were reconstituted in 90 µl of 50 mM HEPES at pH 8.0. Purified protein was quantified as described above. The protein recovery efficiency was determined by comparison of total protein by bicinchoninic acid assay after the initial solubilization step and after purification. A percentage protein recovery was calculated, and conversion from units of femtomoles of peptide per microgram total protein to femtomoles of peptide per litre of seawater was conducted using the recovery efficiency and the total protein quantities. Trypsin (Promega) dissolved in HEPES at pH 8.0 to a concentration of 0.5 µg µl^{-1} was added to samples at a 1:25 trypsin to protein ratio and incubated at 37 °C overnight.

Peptide recovery and preparation. Acetonitrile was added to digested peptides at a concentration of ≥95% and incubated for 20 min at room temperature. Samples were then placed on the magnetic rack for 2 min and supernatant was removed and discarded. Acetonitrile (1,400 µl) was added to samples on the magnetic rack for 15 s. Supernatant was removed and discarded. Samples were air dried for approximately 4 min, just until acetonitrile was evaporated. Beads were reconstituted in 90 µl of 2% DMSO and incubated off the rack at room temperature for ≥15 min. Samples were centrifuged slowly and briefly at a relative centrifugal force of 900 to remove liquid from the tube walls. Samples were incubated on the magnetic rack for 15 min and supernatant containing peptides was transferred to a new ethanol-washed 1.5-ml microtube. This step was repeated to insure removal of all magnetic beads. 1% trifluoroacetic acid was added to samples for a final concentration of 0.1%. Samples were zip tipped with Pierce C18 tips according to the manufacturer's protocol with a final resuspension in 25 µl of 70% acetonitrile, 0.1% formic acid. Samples were evaporated to approximately 10 µl in a DNA110 SpeedVac (Thermo Savant). Samples with lower protein concentrations were further evaporated to minimize the acetonitrile percentage in the final resuspension–zip tip product to be less than 30% of the total final buffer B volume. Samples were finally resuspended to a peptide concentration of 1 µg µl^{-1} in buffer B (2% acetonitrile, 0.1% formic acid).

Global metaproteome mass spectrometry. Global metaproteomic analyses were conducted using one-dimensional and two-dimensional chromatographic separation for the Metzyme and ProteOMZ expeditions respectively. Following global metaproteomic analyses, targeted metaproteomic assays were designed and samples were analysed again by PRM mass spectrometry using mass spectral information from the global proteomic analyses.

One-dimensional global proteomes were analysed with a Thermo Fusion mass spectrometer and a Michrom Advance HPLC with a Thermo Flex source. For each sample, 1 µg (measured before trypsin digestion) was concentrated onto a trap column (200 µm × 10 mm inner diameter, 5-µm particle size, 120-Å pore size, C18 Reprosil Gold, Dr. Maisch) and rinsed with 100 µl of 0.1% formic acid, 2% acetonitrile, 97.9% water before gradient elution through a reverse-phase C18 column (100 µm × 400 mm inner diameter, 3-µm particle size, 120-Å pore size, C18 Reprosil Gold, Dr. Maisch) at a flow rate of 300 nl min^{-1}. The chromatography consisted of a nonlinear 200-min gradient from 5% to 95% buffer B, where A was 0.1% formic acid in water and B was 0.1% formic acid in acetonitrile (all solvents were Fisher Optima grade). The mass spectrometer was set to perform scans on the Orbitrap (240,000 resolution at 200 *m*/*z*, mass to charge ratio) with a scan range of 380 *m*/*z* to 1,580 *m*/*z*. MS2 scans were performed on the ion trap using data-dependent settings (top speed, dynamic exclusion 15 s, excluding unassigned and singly charged ions, precursor mass tolerance of ±3 ppm, with a maximum injection time of 150 ms).

Two-dimensional global proteomes were analysed with a Thermo Fusion mass spectrometer following online two-dimensional active-modulation liquid chromatography using a Dionex Ultimate3000 RSLCnano system with an additional RSLCnano pump. The first column separation utilized a nonlinear 8-h pH = 10 gradient (10 mM ammonium formate in water and 10 mM ammonium formate in 90% acetonitrile) on a PLRP-S column (200 µm × 150 mm, 3-µm bead size, 300-Å pore size, NanoLCMS Solutions). The eluent was diluted inline (10 µl min^{-1} of 0.1% formic acid) then trapped and eluted every 30 min on alternating dual traps (300 µm × 5 mm, 5-µm bead size, 100-Å pore size, C18 PepMap100, Thermo Scientific). The alternating traps were eluted at 500 nl min^{-1} onto a C18 column (100 µm × 150 mm, 3-µm particle size, 120-Å pore size, C18 Reprosil Gold, Dr. Maisch, packed in a New Objective PicoFrit column) with a 30-min nonlinear gradient (0.1% formic acid in water and 0.1% formic acid in 99.9% acetonitrile) on a Thermo Flex ion source attached to the mass spectrometer. Fusion scan settings were set to 240,000 resolution and 380–1,580 *m*/*z* for MS1 scans in the Orbitrap. MS2 scans had a 1.6-*m*/*z* isolation window at normal scan rate, 50-ms maximum injection time, collision-induced dissociation activation and a 5-s dynamic exclusion in the ion trap.

Global metaproteomic data analysis. The raw mass spectrum files were searched using SEQUEST HT within Thermo Proteome Discoverer 2.1 software using a parent ion tolerance of 10 ppm and a fragment tolerance of 0.6 Da. Processed files were then loaded into Scaffold 4.8 (Proteome Software) with a protein threshold of 99.0% and a custom peptide threshold (0.95 probability and SEQUEST XCorr values of at least 1.8, 2.5, 3.5 and 3.5 for XCorr (+1), (+2), (+3) and (+4) respectively, and DeltaCN of at least 0.1). Peptide and protein false discovery rates (FDR) were 0.1% and 1.6%, respectively, against a decoy database, for exclusive and total spectral count outputs. Protein and peptide reports as well as FASTA files were exported and submitted to BCO-DMO and the Ocean Protein Portal.

Targeted metaproteomics: synthesis and calibration of peptide standards, and mass spectrometry. Tryptic peptides from the Nxr alpha (seven peptides) and beta (five peptides) subunits were targeted for absolute quantitation (Supplementary Table 2). Peptides containing methionine and cysteines were avoided whenever possible, although one from each subunit contained these residues. All peptides were discovered in metaproteomic data-dependent analyses before targeting to confirm their ability to extract, digest and ionize efficiently. Absolute calibration of peptides was conducted using a modified QconCAT approach[57], where custom-designed stable-isotope-labelled peptides were heterologously produced in *Escherichia coli* by synthesized DNA with six-amino-acid spacer regions between targeted peptides and ligated into a PET-30a overexpression vector (Novagen) grown in ^{15}N-labelled lysogeny broth growth medium (Cambridge Isotopes) to produce fully ^{15}N-labelled heavy peptides. The labelled peptides were calibrated relative to commercially available peptides (for example, Pierce BSA, apomyoglobin) by direct ratio measurement against the unknown-plasmid labelled peptides. For example, 2 µl of Pierce peptides (500 fmol µl^{-1}) were added to 10 µl of digested labelled peptides and brought up to 100 µl in carrier solution, and 10 µl were injected into the mass spectrometer. The ratio of Pierce to identical labelled sequences in the plasmid was determined, and using the known concentration of unlabelled Pierce peptide sequences the concentration of the ^{15}N-labelled Pierce peptide sequence was determined. Because isotopically labelled standard peptide sequences within each plasmid were stoichiometric, 1:1, with target

peptide sequences, their absolute abundance in the sample was determined by multiplying by the ratio of labelled versus unlabelled standard peptide sequences and subsequent volume corrections.

PRM targeted metaproteome analyses were also conducted on the Thermo Orbitrap Fusion. Samples were injected onto a trap column (300 µm × 5 mm, 5-µm bead size, 100-Å pore size, C18 PepMap100, Thermo Scientific) at 10 µl min^{-1} and washed for 10 min with 0.1% formic acid in 2% acetonitrile. The trapped sample was then eluted at 500 nl min^{-1} onto a C18 column (100 µm × 150 mm, 3-µm particle size, 120-Å pore size, C18 Reprosil Gold, Dr. Maisch, packed in a New Objective PicoFrit column) with a 70-min nonlinear gradient (0.1% formic acid in water and 0.1% formic acid in 99.9% acetonitrile) into the mass spectrometer. PRM settings in the Fusion were set to 240,000 Orbitrap resolution at a scan range of 350–1,200 *m/z* for MS1, and a targeted mass list (Supplementary Table 3) in the ion trap with collision-induced dissociation activation in normal scan rate mode with a maximum injection time of 35 ms for MS2 scans.

Standard curves for the labelled standards were examined for linearity, and those with low linearity (low linear regression r^2 values) were excluded from the study (Supplementary Table 2 and Supplementary Fig. 8). The precision of technical replicates for this suite of 12 targeted peptides on three samples revealed relative s.d. values of 6.2%, 6.2% and 3.9% (Supplementary Table 4).

Taxonomic analysis of targeted peptides. The taxonomic attribution of the targeted tryptic peptides and full protein sequences was conducted to identify their microbial source using the METATRYP software[58]. A database of tryptic peptides from marine microbes was constructed from genomes and representative NOB single amplified genomes, and the occurrence of our tryptic peptide targets among marine microbes was examined, as previously done for species and ecotype-level differentiation on the well characterized marine cyanobacteria (Supplementary Tables 5 and 6). A METATRYP database was constructed containing over 300 marine microbial genomes, including some representative single amplified genomes, and was queried for the presence of the targeted peptides. Of the 12 peptides, 11 were taxonomically attributed exclusively to the NOB *Nitrospina* sp., with the 12th peptide present in both *Nitrospira* and *Nitrospina* (Supplementary Tables 5 and 6), by least common ancestor analysis using representative NOB genomes and single amplified genomes.

NOB cultivation and global proteomic analyses. The NOB *N. marina* Nb-295 and *N. mobilis* Nb-231 were grown in batch cultures in autoclaved medium prepared with 75% natural seawater and 25% ultrapure water with 400 µM $MgSO_4$, 30 µM $CaCl_2$, 5 µM K_2HPO_4, 2.3 µM Fe III ethylenediaminetetraacetic acid, 0.1 µM Na_2MoO_4, 0.25 µM $MnCl_2$, 0.002 µM $CoCl_2$, 0.08 µM $ZnSO_4$ and 2 mM $NaNO_2$ (ref. [3]). For Nb-295, after the initial 2 mM NO_2^- was exhausted, cultures were fed an additional 2 mM NO_2^-. Cultures were grown at 22 °C in the dark in 500 ml polycarbonate bottles without shaking.

Samples were resuspended with 1,800 µl of 1% SDS extraction buffer (1% SDS, 0.1 M Tris/HCl at pH 7.5, 10 mM EDTA). Each sample was incubated at room temperature for 15 min, heated to 95 °C for 10 min and shaken at room temperature, 350 r.p.m. for 1 h. The protein extracts were decanted and centrifuged at 14,100 *g* (14,500 r.p.m.) for 20 min at room temperature. The supernatants were removed and concentrated by membrane centrifugation to approximately 300 µl in 6-ml, 5,000 MWCO Vivaspin units (Sartorius Stedim). Each sample was precipitated with cold 50% methanol, 50% acetone, 0.5 mM HCl for 3 d at −20 °C, centrifuged at 14,100 *g* for 30 min at 4 °C, decanted, and dried by vacuum concentration (Thermo Savant SpeedVac) for 10 min or until dry. Pellets were resuspended in 1% SDS extraction buffer and left at room temperature for 1 h to completely dissolve. Total protein was quantified (Bio-Rad DC protein assay) with BSA as a standard and purified by tube gel purification as described previously[32,59], and global proteomes were analysed on a Fusion Orbitrap mass spectrometer using one-dimensional nanospray separation and topN data-dependent acquisition as described above.

Absolute protein abundance-based enzyme activity estimates. Estimates of maximal possible in situ reaction rates were conducted using the published specific activities for purified Nxr from *Nitrobacter hamburgensis* of 2,506 and 1,740 units mg^{-1} min^{-1} for nitrite oxidation and nitrate reduction, respectively, where one unit represents 1 nmol NO_3^- formed or consumed per minute[34]. Using the average of the NxrA and NxrB abundances at Metzyme station 3 maxima of 131 fmol l^{-1} (average of 107 and 155 fmol l^{-1} = 131 fmol l^{-1} NxrAB; 131 kDa and 49 kDa molecular masses; assuming 1:1 NxrA:NxrB) yielded 23.6 ng l^{-1} of enzyme (5.6 fmol l^{-1} = 1 ng l^{-1}). Equations (1) and (2) provide the potential maximal reaction rates for nitrite oxidation and nitrate reduction, respectively.

$$24\,\mathrm{ng\,l^{-1}} \times 2{,}506\,\mathrm{nmol}\,\frac{\mathrm{NO_2\ oxid.}}{\mathrm{mg\,min}} \times \frac{1\,\mathrm{g}}{1\times10^9\,\mathrm{ng}} \times \frac{1\times10^3\,\mathrm{mg}}{\mathrm{g}} \times \frac{60\,\mathrm{min}}{\mathrm{h}} \times \frac{24\,\mathrm{h}}{\mathrm{d}} = 85\,\mathrm{nM\,d^{-1}} \quad (1)$$

$$24\,\mathrm{ng\,l^{-1}} \times 1{,}750\,\mathrm{nmol}\,\frac{\mathrm{NO_3\ red.}}{\mathrm{mg\,min}} \times \frac{1\,\mathrm{g}}{1\times10^9\,\mathrm{ng}} \times \frac{1\times10^3\,\mathrm{mg}}{\mathrm{g}} \times \frac{60\,\mathrm{min}}{\mathrm{h}} \times \frac{24\,\mathrm{h}}{\mathrm{d}} = 59\,\mathrm{nM\,d^{-1}} \quad (2)$$

More refined nitrite oxidation rates were then calculated using Michaelis–Menten parameters from NOB cultures (Supplementary Table 6) including *N. moscoviensis*[47] and *N. watsonii*[46]. *N. moscoviensis* was isolated from pipes in built environments, and hence kinetic parameters based on a more representative nitrifier, *N. watsonii*, were used for vertical profiles of Nxr estimated reaction rates. Reaction rate values, *V*, were calculated using environmental nitrite concentration data, including 0.5 µM as a maximum value, as used above, or ambient seawater nitrite concentrations at each corresponding depth (equation 3 and Fig. 1f,g). These *V* values were multiplied by the average NxrAB abundances (converted to ng l^{-1} as described above), and the fraction of Nxr to total cellular protein (F_{Nxr}), to convert literature kinetic parameters normalized to total cellular protein[46] to actual enzyme concentration normalization. F_{Nxr} was set at 0.1 (10%) on the basis of previous protein purification studies[38,60], and was consistent with our preliminary targeted *Nitrospina* culture data.

$$V\left(\frac{\mu\mathrm{mol\,NO_2}}{\mathrm{mg\,h}}\right) = (V_{\max}[\mathrm{NO_2}])/(K_\mathrm{m} + [\mathrm{NO_2}]) \quad (3)$$

$$\mathrm{Rxn\ rate}\left(\frac{\mathrm{nmol}}{\mathrm{dl}}\right) = V\left(\frac{\mu\mathrm{mol\,NO_2}}{\mathrm{mg\,h}}\right) \times \frac{1\times10^3\,\mathrm{mg}}{1\,\mathrm{g}} \times \frac{1\,\mathrm{g}}{1\times10^9\,\mathrm{ng}} \times \mathrm{NxrAB}\left(\frac{\mathrm{ng}}{\mathrm{l}}\right) \times \frac{1}{F_{\mathrm{Nxr}}} \times \frac{24\,\mathrm{h}}{\mathrm{d}} \times \frac{1\times10^3\,\mathrm{nmol}}{\mu\mathrm{mol}} \quad (4)$$

Metagenomic analyses. Splits from the 0.2–3.0-µm fraction of the McLane pump samples from Metzyme 150, 250, 300, 550 and 800 m from station 3 and 50 m from station 5 were extracted for DNA and were submitted to the Joint Genome Institute for metagenomic sequencing. Quality trimmed reads were assembled in a sample-specific fashion using metaSPAdes and annotated as previously described[61]. The assembly has been deposited in NCBI under accession GCA_900411625.

Nitrate isotopic analyses. The N isotopic composition of nitrate is expressed in delta notation, where $\delta^{15}N = (^{15}N/^{14}N_{sample})/(^{15}N/^{14}N_{reference}) - 1$, referenced to atmospheric N_2 and expressed in ‰ by multiplying by 1,000. Nitrate $\delta^{15}N$ was measured using the denitrifier method[62,63].

Nutrient analyses. Macronutrient samples were collected from the trace metal rosette and filtered though 0.2-µm filters, frozen and analysed as previously described[64]. N* was calculated as previously described ($N^* = (NO_3 - 16PO_4 + 2.9) \times 0.87$) (refs. [21,22]). Dissolved cobalt samples were analysed by cathodic stripping voltammetry after ultraviolet irradiation, as previously described[65].

N_2O analyses. Samples were collected in glass serum bottles and sealed at sea, and analyses were conducted as described previously[66].

Data availability

Environmental data and processed global and targeted metaproteomic results from Metzyme and ProteOMZ expeditions are available at https://www.bco-dmo.org/ under projects 2236 and 685696 and dataset 806510, and the global metaproteomes can be explored through the Ocean Protein Portal (https://www.oceanproteinportal.org). The metagenomic assembly used for peptide-to-spectrum matching is available at NCBI under accession GCA_900411625. Targeted Nxr concentrations and NOB abundances are available within Supplementary Tables 9 and 8. Raw mass spectra are available in PRIDE and ProteomeXchange as project number PXD009712.

References

56. Hughes, C. S. et al. Ultrasensitive proteome analysis using paramagnetic bead technology. *Mol. Syst. Biol.* **10**, 757 (2014).
57. Brownridge, P. J., Harman, V. M., Simpson, D. M. & Beynon, R. J. in *Quantitative Methods in Proteomics* (ed. Marcus, K.) 267–293 (Springer, 2012).
58. Saito, M. A. et al. Needles in the blue sea: sub-species specificity in targeted protein biomarker analyses within the vast oceanic microbial metaproteome. *Proteomics* **15**, 3521–3531 (2015).
59. Lu, X. & Zhu, H. Tube-gel digestion. *Mol. Cell. Proteom.* **4**, 1948–1958 (2006).
60. Tanaka, Y., Fukumori, Y. & Yamanaka, T. Purification of cytochrome a_1c_1 from *Nitrobacter agilis* and characterization of nitrite oxidation system of the bacterium. *Arch. Microbiol.* **135**, 265–271 (1983).
61. Dupont, C. L. et al. Genomes and gene expression across light and productivity gradients in eastern subtropical Pacific microbial communities. *ISME J.* **9**, 1076–1092 (2015).
62. Sigman, D. et al. A bacterial method for the nitrogen isotopic analysis of nitrate in seawater and freshwater. *Anal. Chem.* **73**, 4145–4153 (2001).
63. Casciotti, K. L., Sigman, D. M., Hastings, M. G., Böhlke, J. K. & Hilkert, A. Measurement of the oxygen isotopic composition of nitrate in seawater and freshwater using the denitrifier method. *Anal. Chem.* **74**, 4905–4912 (2002).

64. Noble, A. E. et al. Basin-scale inputs of cobalt, iron, and manganese from the Benguela-Angola front into the South Atlantic Ocean. *Limnol. Oceanogr.* **57**, 989–1010 (2012).
65. Hawco, N. J., Ohnemus, D. C., Resing, J. A., Twining, B. S. & Saito, M. A. A dissolved cobalt plume in the oxygen minimum zone of the eastern tropical South Pacific. *Biogeosciences* **13**, 5697–5717 (2016).
66. Westley, M. B., Yamagishi, H., Popp, B. N. & Yoshida, N. Nitrous oxide cycling in the Black Sea inferred from stable isotope and isotopomer distributions. *Deep Sea Res. II* **53**, 1802–1816 (2006).

Acknowledgements

We thank the captain and crews of the RV *Kilo Moana* and RV *Falkor* for their assistance. We appreciate the sampling assistance from T. Goepfert, N. Held, N. Hawco, T. Horner, C. Hau, and D. Wang. Metagenome and *N. marina* sequencing was provided by the Department of Energy Joint Genome Institute. Time aboard the RV *Falkor* was provided by the Schmidt Ocean Institute. Funding for this research in the Saito laboratory was provided by the Gordon and Betty Moore Foundation (3782) and the National Science Foundation (OCE-1031271, 1736599, 1657766, 1850719, 1924554). J.K.S. was supported by the NASA Postdoctoral Fellowship Program. A.E.S. was supported by the Sloan Foundation, the Simons Foundation and United States National Science Foundation award OCE-1437310. A portion of this research used resources at the DOE Joint Genome Institute sponsored by the Office of Biological and Environmental Research and operated under contract DE-AC02-05CH11231 (JGI). C.L.D. and D.K. were supported by NSF grant OCE-1259994.

Author contributions

M.A.S. led field expeditions, collected samples, analysed datasets and wrote the manuscript. M.R.M. analysed samples by mass spectrometry and developed targeted proteomic assays. D.M.M. collected and extracted metaproteomic samples. A.E.S. participated in the expeditions, contributed to interpretations, measured NOB abundances, cultured Nb-295 and edited the manuscript. C.L.D. analysed metagenomics datasets, provided metagenomic assemblies and contributed to the manuscript. P.A.R. analysed $^{15}N\text{-}NO_3$ samples and contributed to the manuscript discussion. J.K.S. contributed to metaproteomic informatic analyses and manuscript interpretations. D.K. contributed to metagenomic informatic analyses. M.W. contributed N_2O and nitrite data from KM0405. C.H.L. co-led the Metzyme field expedition, collected samples and contributed to the manuscript discussions. J.B.W. and F.V. contributed to nitrifier culture experiments and manuscript discussions.

Competing interests

The authors declare no competing interests.

Additional information

Supplementary information is available for this paper at https://doi.org/10.1038/s41561-020-0565-6.

Correspondence and requests for materials should be addressed to M.A.S.

Peer review information Primary Handling Editor: Rebecca Neely.